Optimization of the parameters in the electronics of a PET detector.

(Optimización de los parámetros de la electrónica de un detector para PET)

Ana María Barragán Montero

July 4, 2013

UNIVERSIDAD COMPLUTENSE
MADRID

Academic project (TAD, Trabajo Académicamente Dirigido).
Departamento de Fsica Atmica, Nuclear y Molecular.

Supervised by:
Dr. Jose Manuel Udías Moinelo. (Director)
Esteban Picado Sandí (Co-Director)
Jacobo Cal González (Co-Director)

Contents

Motivation and acknowledgements

Some months ago I started the final year of my degree in Physics and I wanted to do something different, something more practical and exciting than a common subject in the course. Indeed, I wanted to be closer to research world and work by my own, so I decided to try a supervised project (TAD, trabajo acaémicamente dirigido). I chose the Atomic and Nuclear Physics Department because I became very interested in nuclear physics. I have to thank Jose Manuel Udías for being always ready to supervise and direct my project in any of the topics which I considered. At the beginning I had in mind a very different topic, a more theoretical one (' electron scattering by nuclei'), however, I realised that I needed to do something more applied. I began then with my project about PET. Now, I am very happy I decided to do this work and that I chose this topic because I feel I learnt a lot. I have learnt a lot about PET but also, and even more important, about programming, data analysis and processing, Linux, Fortran, gnuplot,... At the end, I have developed a lot of new and good skills making me a better scientist. I can say it has been totally worth it :)

I want to thank Esteban Picado for his help at the beginning, when I was a bit lost about what to do, for showing me the way to start and how to reach the important points in the project. I also want to thank Jacobo Cal for always being ready to answer any question or helping me with the program codes, and all the people in the laboratory for maintaining always such a good atmosphere.

To finish, I want to dedicate this work to all my close friends during these five years of my degree, for being always there, making me happy, they know who they are.

1. Introduction

PET (Positron Emission Tomography) is a medical imaging technique based on the beta-decay mechanism by positron emission (β^+ decay) of some radioactive elements. Thus, in order to use this technique to study a body it is necessary to introduce a positron emitting radionuclide into it.

This radionuclide is the so-called 'tracer' and is introduced on a biologically active molecule to be able to interact with the surroundings in the body.

Two phenomena are essentially important in PET: positron emission and electron-positron annihilation. The theory behind both processes is explained in the following sections, but in short, when an emitted positron (by the tracer) collides with a surrounding electron in the body, the result is the annihilation of both the electron and positron and the creation of two parallel gamma ray photons emitted in opposite directions. These pair of gamma photons are detected in coincidence by the scanner-system and then processed by the electronics and computer analysis to construct images which reproduce the tracer concentration in the body.

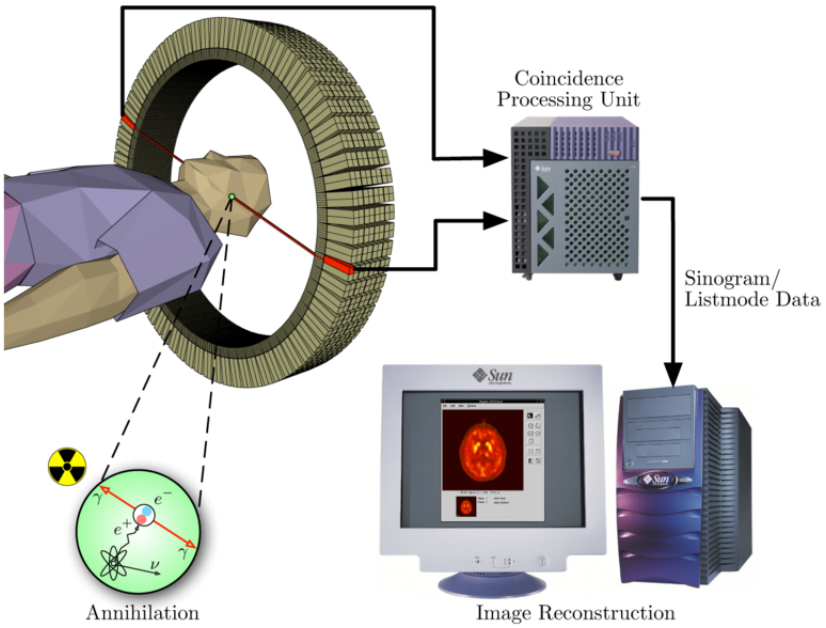

Figure 1: Scheme of the data acquisition process in PET. [11]

Since the tracer concentration is what is being reproduced, PET images are very useful not only to create simple images of a part of the body but also to show the behaviour of the organism by following the tracer path and how certain organs perform their function. This is the main difference between PET and other traditional anatomic imaging techniques such as CT (Computed Tomography).

A typical PET scanner comprises several detector rings which consist of detector blocks like the one shown in Figure 2. The studied subject is placed inside the ring and

the detectors will detect in coincidence the pair of gamma rays emitted by the tracer, so that they define a line of response (LOR) along which the positron annihilation took place. Then, the electronics creates a signal which will be sent to the computer.

This last part, the computer analysis of the pulses generated by the electronics is the one in which this work is focused on.

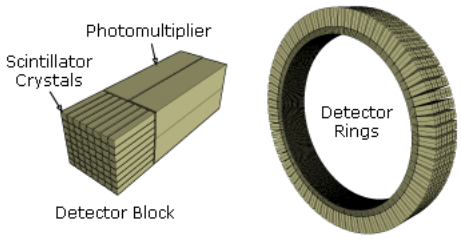

Figure 2: Schematic view of a detector block and a ring scanner. [11]

In particular, our aim is to study which are the conditions that give the best quality for the final image. For that purpose, raw data collected by a single detector will be analyzed and processed with computer programs in order to study which are the best values for certain parameters that give a good quality image. These parameters are discussed in the sections below.

The language in which the programs are created is FORTRAN. One of the main programs is created by Jose Manuel Udías and the rest are created by the author of this work, but always with the help of Jacobo Cal.

2. Physical background for PET

2.1. Beta-decay and $e - e^+$ annihilation

Beta-decay is a process in which a non-stable (radioactive) proton or neutron rich nuclei undergoes a proton or neutron decay in order to reach high stability. Hence, there are two different beta particles depending on which decay occurs. If the nucleus undergoes a neutron decay, (β^- decay), one neutron is transformed into a proton and the emitted beta particle is an electron (and the consequent anti-neutrino) according to the process $n \rightarrow p + e^- + \overline{\nu_e}$.

On the contrary, when a proton decay occurs, (β^+ decay) , one of the protons is transformed into a neutron and the emitted particle is a positron (and a neutrino), $p \rightarrow n + e^+ + \nu_e$.
This last one, (β^+ decay) , is the one in which PET is based on and it cannot happen in free, isolated nuclei due to energy constrains. However, for protons inside a nucleus this decay is sometimes energetically possible and it is written as:

$$X_N^Z \rightarrow X_{N+1}^{Z-1} + e^+ + \nu_e \tag{1}$$

To be more precise, this occurs in nuclei where the decay energy Q is positive, being Q given as:

$$Q = [m(^{A}X) - m(^{A}X') - 2 \cdot m_e]c^2 \tag{2}$$

The available energy in this process is shared between the positron and the neutrino, as a consequence the energy spectrum for the emitted positron is continuous. Typical energy spectrum is shown in Figure 3.

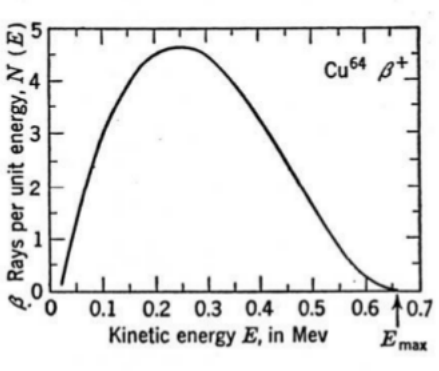

Figure 3: Typical energy spectrum for β^+ decay. [4]

Thanks to this kinetic energy the positron is able to travel a distance since it is emitted until it loses all the energy. When they travel, they interact with the surrounding matter losing its energy. After losing enough energy, the positron will annihilate with a nearby electron:

$$e^+ + e^- \rightarrow \gamma + \gamma \tag{3}$$

In this positron-electron annihilation process 4, energy and momentum are conserved and two gamma rays are emitted in opposite directions defining a LOR (line of response), each having an energy equal to the rest of mass of the electron (or positron) 511 keV.

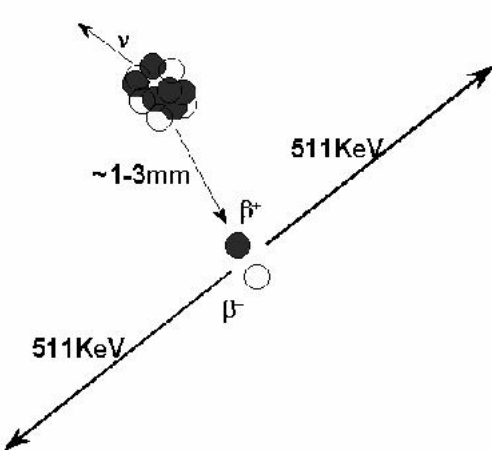

Figure 4: Positron-electron annihilation process.[12]

2.2. Positron range

The distance from the emission point to the annihilation point is called 'positron range' and depends on both the energy of the emitted positrons and the surrounding material. Positron range is one of the main limiting factors to the spatial resolution in PET.

Other interesting concept, relevant for projection data, is the 'positron blurring', which is the distance from the decaying atom to the LOR in the normal direction.

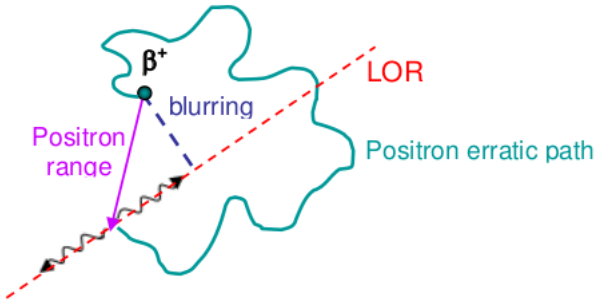

Figure 5: Positron blurring effect. [6]

2.3. Interaction of gamma radiation with matter

This section constitutes a brief explanation of the different ways that gamma rays can interact with matter, and therefore a help to understand how the two gamma rays emitted after the annihilation process will interact with the detectors in the scanner.

Gamma rays which fall inside the range 1keV- 1GeV interact with the matter by three major mechanisms: photoelectric absorption, Rayleigh or Compton scattering and pair production.

2.3.1. Photoelectric absorption

In photoelectric absorption the gamma ray loses all of its energy in one interaction.

The incident gamma ray with energy E_γ is absorbed entirely by an atom in the matter and an electron from the shell is then ejected with energy $E_{e^-} = E_\gamma - E_{bound}$, where E_{bound} is the binding energy of the emitted electron, which is called 'photo-electron'.

The probability of photoelectric absorption depends on the gamma-ray energy, the electron binding energy and the atomic number A of the atom. Therefore, the photo-electric mass attenuation coefficient can be given by $\tau \propto \frac{Z^4}{E^3}$.

2.3.2. Rayleigh and Compton scattering

Both mechanisms are scattering processes, however, elastic scattering is known as Rayleigh scattering while inelastic scattering is known as Compton.
In an elastic (Rayleigh) scattering a gamma ray with energy E_γ interacts with a shell electron and is deflected from its incident direction without changing its energy.

When Compton scattering occurs, the gamma ray with energy is deflected by an angle θ and it also loses energy which is transferred to the electron E_{e^-}.

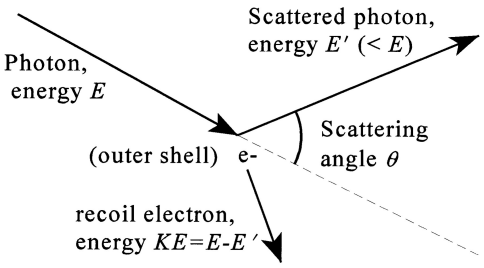

Figure 6: Compton scattering. [13]

Thus, the gamma ray left with an energy $E_\gamma^{'}$ after the interaction which can be simply calculated by applying conservation of momentum as $E_{e^-} = E_\gamma - E_{bound} - E_\gamma^{'}$.

The energy $E_\gamma^{'}$ depends on the scatter angle θ and this dependence is given by:

$$E_\gamma^{'} = \frac{E_\gamma}{1 + \frac{E_\gamma}{m_e c^2}(1 - \cos\theta)} \tag{4}$$

There exists a situation which sets the maximum energy transferred to the electron and gives rise to the so-called 'Compton edge' in the energy spectrum of gamma rays. This happens for $\theta = \pi$.

2.3.3. Pair production

Pair production process occurs when a photon is transformed into a pair electron-positron. It is only possible for gamma rays with energy above twice the energy of electron (positron), that is, 1.022 MeV (2x511 keV). Moreover, the interaction can only take place in the presence of a nucleus to pick up the recoiling energy and momentum. At the range of energies used in PET (511 keV), pair production is not energetically possible so it will not be relevant in our study.

Therefore, the two main ways of interaction in PET are photoelectric absorption and Compton scattering. In order to have a high resolution the photons must leave all the energy in only one crystal and in one interaction, that is, photoelectric absorption is the preferred interaction in PET.

3. Detectors

Once the mechanisms by which the gamma rays are created and the way that the energy is left in the crystal are explained, the next step is to understand how these gamma rays

are detected.
In figure 2, a typical scheme for a PET scanner is presented, together with a detector block. As it is shown in the figure, a scintillation detector consists of a block of scintillation crystal assembled to a photomultiplier (PMT). When the incident radiation interacts with the crystal, it produces scintillation light which is amplified and converted into an electrical signal by the PMT.

3.1. Scintillators

Scintillation materials are materials which are able to absorb gamma radiation and re-emit it in form of visible light.

Detectors in PET are made of scintillation material because they may be very fast, can have high stopping power and exhibit low electronic noise when coupled to PMTs. Moreover, as it was explained before, the preferred interaction is the photoelectric absorption since it produces a single scintillation center.

On the contrary, in Compton scattering the scattered photon can produce several interactions and therefore several scintillation centers which cause problems when determining the position.

In order to be a good detector, scintillators must have then high density (for a high absorption probability) and high atomic number for a large fraction of photons undergoing photoelectric absorption. High light yield is also required, that means that a large fraction of the emitted scintillation photons should be detected.

Scintillation materials can be organic-based or inorganic. In PET scans, inorganic ones are usually used since they have a higher light yield, although organic ones are faster.

	NaI(Tl)	BaF_2	LSO	GSO	LYSO	$LaBr_3$	LFS	LuAP	LuI_3
Effective atomic no. (Z)	51	54	66	59	60	47	63	65	60
μ (cm^{-1})	0.34	0.44	0.87	0.62	0.86	0.47	0.82	0.9	~0.56
Density (gm cm^{-3})	3.67	4.89	7.4	6.7	7.1	5.3	7.3	8.34	5.6
Index of refraction	1.85	-	1.82	1.85	1.81	1.88	1.78	1.95	-
Light yield (% NaI(Tl))	100	5	75	30	80	160	77	16	190
Peak wavelength (nm)	410	220	420	430	420	370	430	365	470
Decay constant (ns)	230	0.8	40	65	41	25	35	18	30
Hygroscopic	yes	slight	no	no	no	no	no	no	yes

Figure 7: Properties of some scintillators used in PET detectors.[1]

3.2. Photomultipliers tubes PMT

As mentioned before, the scintillating crystal is coupled to a photomultiplier tube (PMT) housed in a metallic shield. The aim of the PMT is to amplify the incoming signal coming from the interaction in the crystal. They can multiply the current produced by the incident light in multiple dynode stages and thus allowing individual photons to be detected when the incident flux of light is very low.

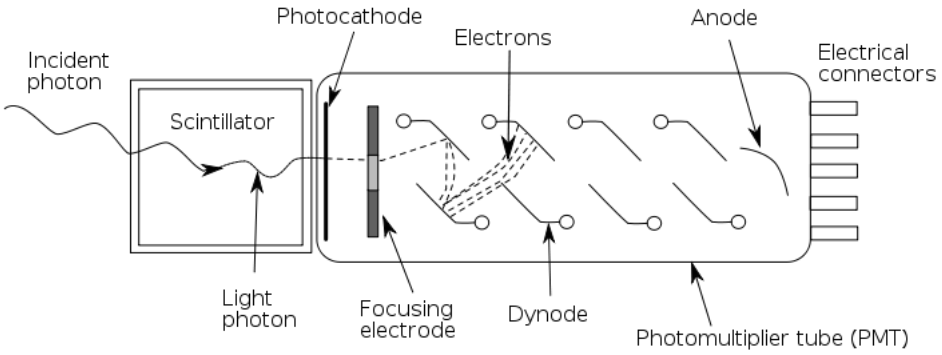

Figure 8: Photomultiplier tube. [14]

PMTs consist of a glass vacuum tube which houses a photocathode, several dynodes and an anode. The incident photons strike the material in the photocathode and electrons are produced due to the photoelectric effect. The electrons arrive to the focusing electrode and are redirected towards the set of dynodes, which is called 'electron multiplier' because it is where the amplification is produced.

Each dynode is just an electrode which experiments a voltage. The voltage increases from one dynode to another, that is, each dynode have a more positive voltage than the previous one. Thus, the electrons striking the first dynode produce new photoelectrons which are accelerated by the electric field created between the dynodes. This process is repeated in each dynode producing a high number of electrons arriving to the final anode.

Finally, the accumulation of charge in the anode results in a current pulse which indicates the arrival of a photon at the photocathode and is proportional to the energy left in the scintillation crystal. These pulses are the aim of study of the present work, as mentioned before they will be processed and analyzed to find the conditions which gives the best quality and image resolution.

Regarding the efficiency of a PMT the concept of 'gain' is defined as the total number of electrons arriving to the anode for each single electron produced in the photocathode. This concept is very important when talking about PS-PMT (position sensitive photomultipliers).

PS-PMT are used to improve the spatial resolution in PET and they consist of scintillation arrays of crystals coupled to a single PMT with an array of anodes where the charge is collected and distributed. The distribution of charge among the different anodes can be used to calculate the point where the interaction takes place. However, it is very usual for anodes to have different gains and that must be taken into account when processing the data. As it will be explained in next sections, this is the reason why our spectra for a single crystal must be individually calibrated in order to be added up to find a final spectrum.

4. Influence of acquisition and processing factors on image quality

There are several factors which can degrade the final image obtained by PET analysis. Thus, these factors must be studied carefully in order to find the optimum value which gives the best image quality. Some of them can be already minimized by means of the scanner system before the data acquisition process. In the present work, the method followed will be done in the other way around, that is, the corrections will be made after the acquisition process, by studying which are the conditions for which our set of data gives the best image quality.

In the following, some of these factors are presented.

4.1. Positron range

As it was explained before (section 2.2), the positron travels a distance called 'positron range' from the point at which it was emitted to the point at which the annihilation takes place. This distance depends on the surrounding matter and the initial energy of the positron, and can take values up to several millimeters. In short, the gamma rays detected by the scanner (LOR) are not produced in the same point where the nucleus decay took place. Hence, by having data about the tissues and the matter of study, positron range can be corrected or at least minimized.

4.2. Non-collinearity

The majority of annihilations take place when the positron has lost almost all the energy and the momentum is nearly zero, at this stage both positron and electron are at thermal energies. However, there exists a probability in which the annihilation occurs with non-zero momentum in the laboratory system, and the emitted gamma rays suffer a slight deviation from 180. This will cause errors in the identification of the annihilation point and therefore will affect the spatial resolution The angular distribution has been measured for this effect and corresponds to a Gaussian distribution with $0.4\text{-}0.5^o width$.

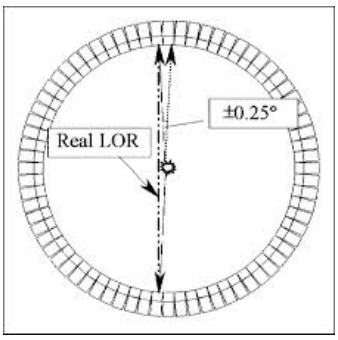

Figure 9: Non-collinearity effects on the LOR.[15]

4.3. Scattering and interaction with several crystals. Crystal identification (Anger logic)

As explained before (section 3.1), the scintillator consists of an array of crystals which is coupled to the PMT.

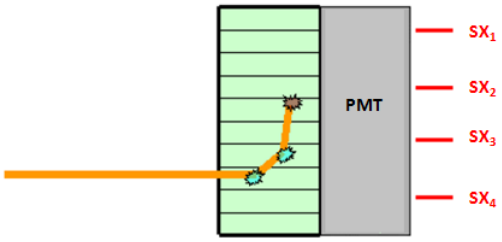

Figure 10: Gamma ray arrives to the scintillator block and interacts in several crystals due to Compton scattering.

The incident photon arriving to the scintillator can leave the energy in a single photoelectric interaction but it can also produce interactions in several crystals by Compton scattering. If several Compton interaction occurs, the energy is then distributed in several crystals which complicates the crystal identification.

The identification of the crystal at which the interaction took place is then made by 'Anger-like logic'. The method takes the name from H.O. Anger [3], who invented the Anger camera in 1957. The method is useful when PS-PMT (position photomultiplier) with multiple anodes are used.

The location of the interaction is determined by processing the voltage signals from the PMT. The position of each anode is weight by the strength of its signal and then a mean position from the weighted position is calculated. The sum of every signal corresponds to the energy left in the crystal $E = \Sigma X + \Sigma Y$.

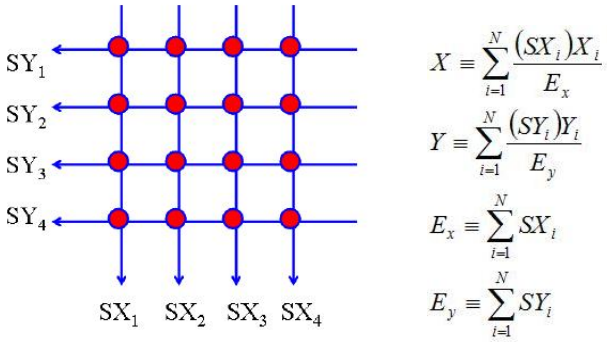

Figure 11: Illustration for anger logic method in a general case.

By representing these mean values for the interaction points, known as 'x, y anger points', the so-called 'flood field maps' are obtained. This kind of maps represents the distribution of the counts in the crystals.

In the particular case or this work, an array of 13x13 crystals coupled to a PS-PMT with four anodes is used. Therefore, the x, y anger points are calculated in the following way:

$$x_{anger} = \frac{X_A - X_B}{X_A + X_B};\ y_{anger} = \frac{Y_A - Y_B}{Y_A + Y_B} \tag{5}$$

and the total energy left in the crystal will be $E = X_A + X_B + Y_A + Y_B$.

Figure 12 represents one the flood field map obtained. It can be noticed that there are exactly 13x13 point-like regions which corresponds to the 169 crystals of our detector.

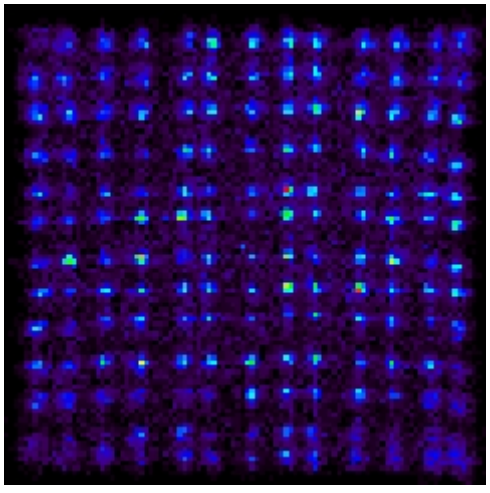

Figure 12: Flood field map from the calculated values for x, y anger.

4.4. Pile-up and dead time

Dead time is defined as the time after each event during which the system is not able to detect another event. As a consequence, the higher the rate of photons hitting a detector, the higher the probability of missing a photon. This problem becomes very important in coincidence detection since both photons must be detected. Dead time losses are minimized by systems with many independent detectors or with faster scintillators and processing electronics.

Pile-up events occurs when a gamma ray is being integrated and an extra gamma ray deposits its energy in the same detector. Pile up events cause two types of errors in PET data. The first one occurs when the pile up event provides a large enough signal to fall outside the energy window and the event is lost. Under this situation, dead time corrections will be required for quantitative measurement. The second error is the partial or total overlapping of both pulses and spatial information will be lost. This affects the energy resolution and the posterior crystal identification process. Again, as a consequence the quality of the image will decrease.

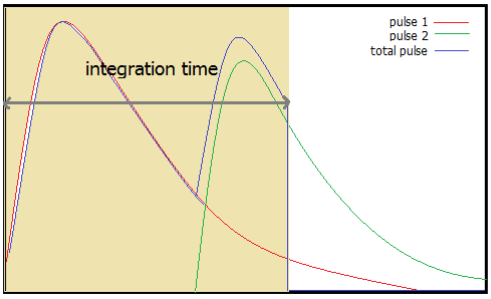

Figure 13: Integration of a pulse with pile-up.

Pile-up effects occurs for high activity acquisitions, high sensitivity scanners and high size detectors red by the same electronics channel, so that the probability to find two coincidences very close in time is very large.
Pile-up can be minimized by reducing the integration time. However, if the integration time is too short, the total charge integrated will be small and the signal to noise ratio will be also poor. Therefore, an optimum value for integration time must be found, keeping an equilibrium between pile-up effects and enough signal to noise ratio.

This study to optimize integration time constitutes a part of this work. For this purpose, our pulses are integrated and analyzed for different integration times trying to figure out which one is best.

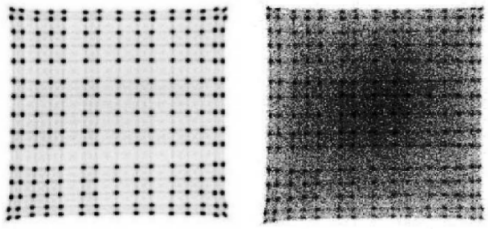

Figure 14: Simulated flood field map for a detector of 15x15 crystals with (right) and without (left) pile-up events. [7]

In figure 14 it can be observed how pile-up effects cause the overlapping of valid coincidence events and therefore a transfer of counts between image planes, leading to loss of counts in the originating plane and additional background events in the destination plane.

4.5. Energy resolution

Energy resolution gives the precision of the system in determining the energy deposited by the incident photons and is usually given by the FWHM of the photopeak of the measured spectrum. The expression used to calculate it is,

$$FWHM = \frac{\Delta E}{E_\gamma} \tag{6}$$

where E_γ is the position for the peak maximum and ΔE is the difference between the two extreme values of the peak at medium height.

A small value for FWHM means that the system is able to distinguish between two events very close in energy, so the smaller FWHM the better energy resolution.

In scintillation detectors, energy resolution depends on the light output of the scintillator, as well as its intrinsic energy resolution which is due to non-statistical effects, such as inhomogeneities in the light yield across the crystal, as well as intrinsic non-linearity of the light conversion process. A good energy resolution is necessary in PET in order to achieve good image contrast and to reduce background (scatter) counts.

4.6. Depth of interaction (DOI)

This problem is illustrated in Figure 15(b). If the source is not in the center of the scanner the effective width of the detector increases and this affects the spatial resolution. By determining the point of interaction in the crystal this problem can be solved but, it is very difficult to know with high precision the depth at which the interaction occurs. This constitutes another degrading factor for the final spatial resolution and image quality. The solution to minimize this problem is called 'phoswich technique' and consists on differencing somehow two or more parts of the crystal.

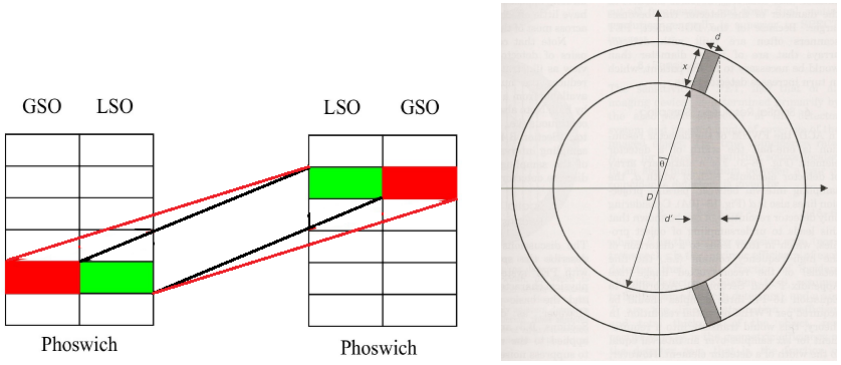

(a) (b)

Figure 15: (a)Picture showing the way in which the phoswich technique reduces the spatial uncertainty when determining the depth of interaction. (b)Illustration of DOI problem, when the source is out of the center of the scanner, the detected photon could be originated in any point inside the gray zone.The effective width of the detector increases when increasing the distance to the center.

There are several types of phoswich, specifically in this work we work with data collected from a two-layer phoswich formed by two different materials LYSO and GSO.

The idea of phoswich relies on the fact that when two scintillators materials optically different are assembled to a PMT, the output pulse will be different depending on the part at which the interaction takes place. Thus, it will be possible to distinguish whether the pulse is coming from one part or from the other.

It is important to choose the scintillators to have difference decay times in order to have a different output pulse. In the following table the decay times for some scintillator materials are presented.

Material	Decay time (ns)
BGO	300
GSO	60
LSO	40
LYSO	40
LuAp	18

Table 1: Decay time for different scintillation materials used in PET.

5. Set-up

5.1. Description of the data set

The data set analyzed in this work was collected with a detector formed by a scintillator block of 169 crystals, that is, a 13x13 array. It is a phoswich detector, which means, as it was explained before in section 4.6, that every crystal is composed by two different layers: the first one is made of LYSO and it is the closest one to the source and the second one is made of GSO.
The scintillator block is coupled to a PS-PMT with four anodes.
The source used was a Sodium-22, which is a positron-emitting isotope with a remarkably long half-life which is usually used to create test-objects and point-sources for PET.

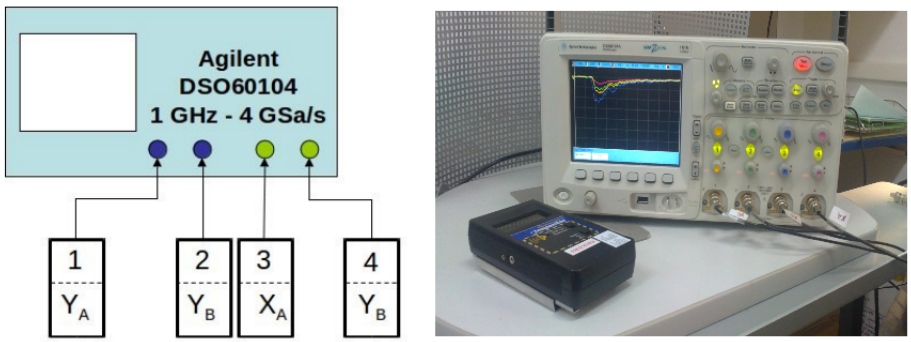

Figure 16: Scheme and picture of the oscilloscope used to acquire the data

Since the multi-anode PMT has several anodes (12 to 64 depending on PMT model),by using the Anger technique and a resistor network, the output of these multiple anodes is combined into just four Anger signales, X1, Y1, X2, Y2. The acquisition process was made with a four channel oscilloscope like the one in Figure 16 (each Anger signal is connected to a channel). Therefore, the final data set will layout as four columns of numbers which represent the output pulses created by each Anger signal when a photon arrives to the scintillator.
Each pulse is sampled with 150 samples and the time between consecutive samples is 1 ns. Therefore, to integrate the entire pulse the integration has to be made up to 150 ns. Shorter integration times can be tried in order to avoid pile-up.

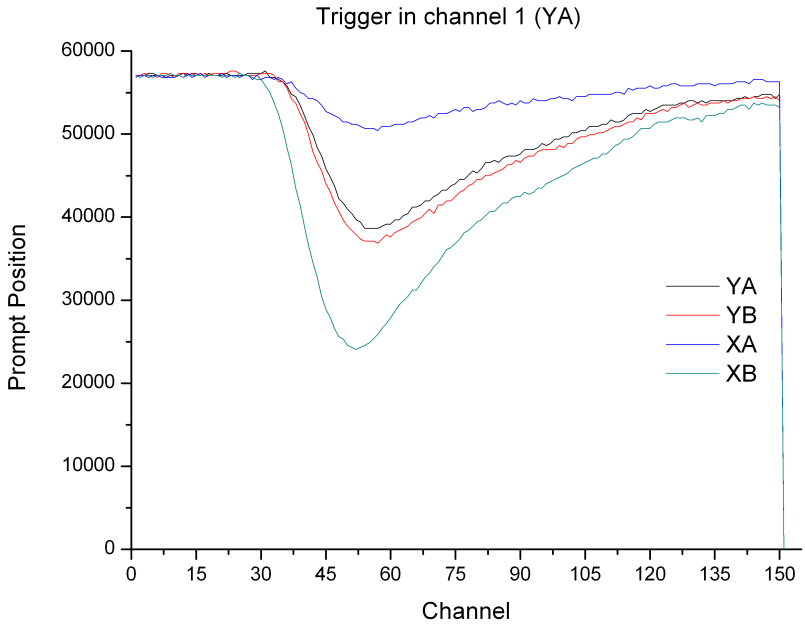

Figure 17: Representation of one of the pulses.

6. Aims of this work

Our first aim is to find the best integration time which minimizes degrading effects such us pile-up and thus gives the best energy resolution and quality image. Once the optimum integration time is known the next step is to find the best phoswich separation, that is, to distinguish between the counts in the first layer (LYSO) and the counts in the second layer (GSO). This will be done by the *delay energy integration method*.

Next task will be the crystal identification process where individual crystals will be selected from the flood field map (x-y anger plot) and the corresponding counts in it will be plotted to make the energy spectrum. From this plot an energy histogram will be built in order to find the energy-channel relationship and then proceed to calibrate each spectrum.

Since the number of counts for individual crystals is quite small, these spectra have not much statistics. Therefore, to conclude this work the final aim is to build an spectrum with more statistics where the sodium photopeak is clearly visible. For this purpose the individual calibrated spectra for LYSO and GSO crystals will be added up separately.

The fact that individual spectra must be calibrated is essential due to each crystal has a difference 'gain' (see section 3.2) and the spectra cannot be added up without a

previous calibration.

Hence, the following steps have been followed:

1 Integration of the pulses (using the program $pulse - procesor.f$ (author Jose Manuel Udías))

2 Phoswich separation. ($phoswich\_total.f$)

3 Crystal identification.($xyanger.f, phoswich\_1crystal.f$). Individual spectra. Histogram and calibration ($histo.f$)

4 Final spectrum. (script $sum\_spectra.sh$)

See appendix A for program code details.

7. Results.

7.1. Pulse integration. Optimum integration time

Based on the program $pulse - procesor.f$, the script $4columns\_procesor.sh$ is created in order to integrate the pulses and find the integrated energy. The complete program code is presented in Appendix A, but the main features are summarized below.

- Pulse-procesor is made for one column data but our data set consists of four columns. Therefore, the script simply runs the program pulse-procesor four times to read and process each column.
- The parameter used to set the integration time is called 'ismax', and the study will be made with several values such as 40, 60, 70, 80, 90, 100 and 150 ns. The value 150 ns constitutes the maximum value for the integration time since our data points are separated 1 ns and there are 150 samples in total in one pulse. The pulses of both LYSO and GSO are well returned to the baseline after 150 ns.

In figure 18 the flood field for each integration time is presented. It can be observed that the quality of the flood field improves with the integration time. More crystal peaks are visible and even more counts seem to be in the figure. This is due to the fact that, with short integration times, there are Anger coordinates of crystals that are outside the 'physics value', due to noise and other reasons.

An equilibrium between enough number of data points and good resolution must be found. From the plots it can be concluded that t=40 ns and t=60 ns can be ignored right away because they do not have good signal to noise ratio to build a good flood field and this will difficult crystal identification.

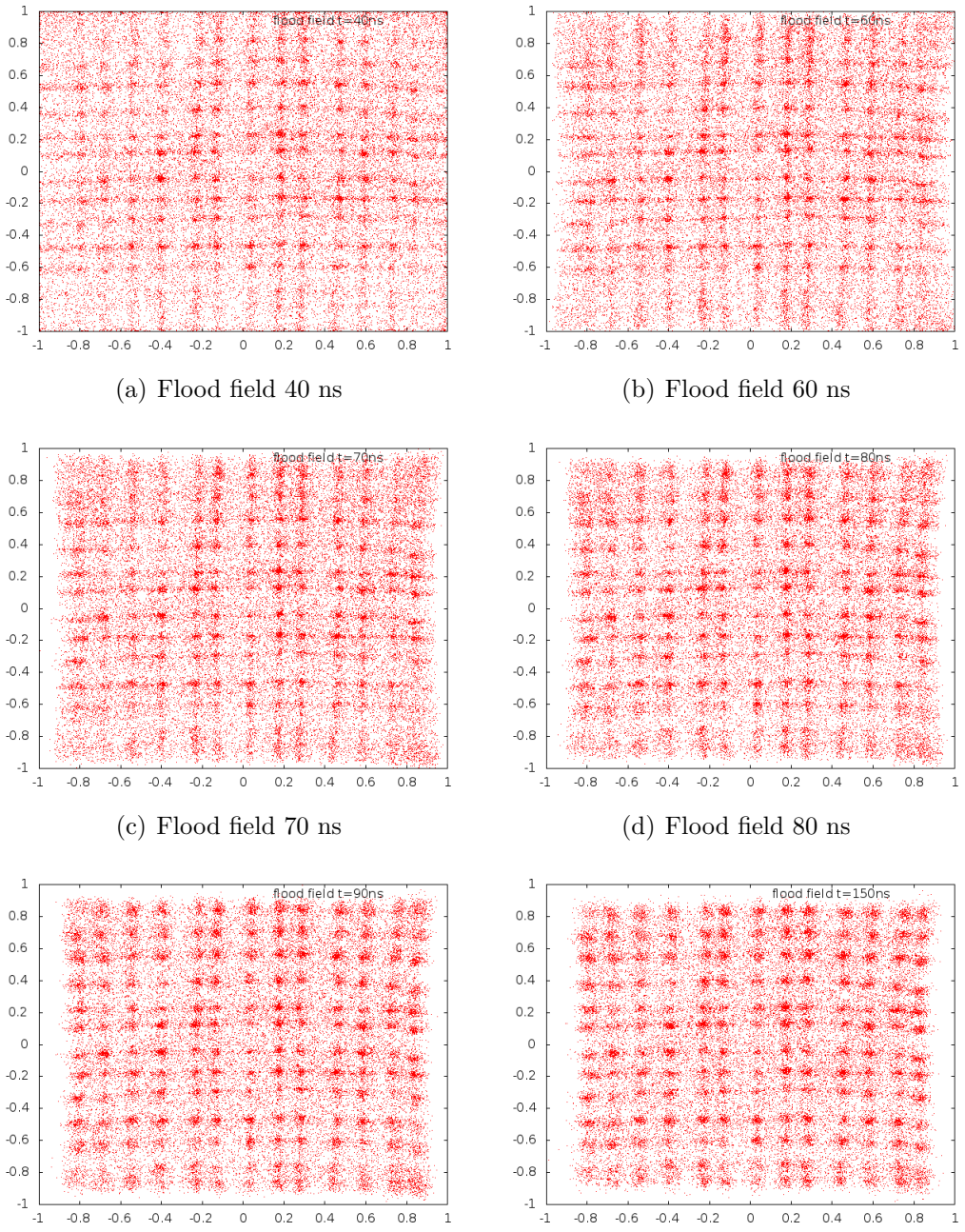

(a) Flood field 40 ns

(b) Flood field 60 ns

(c) Flood field 70 ns

(d) Flood field 80 ns

(e) Flood field 90 ns

(f) Flood field 150 ns

Figure 18: Obtained flood field maps for different integration times.

The analysis is then made over the plots for t=70, 80, 90 and 150 ns. The parameters used to quantify the energy resolution are **FWHM** and the **peak to valley ratio**.

To calculate these parameters the program IMAGEJ [1] is used. This program allows to select individual profiles from the flood field map and then plot them. From these profiles the peak to valley ratio is calculated as the ratio between the arithmetic mean for the maximum values of counts (peaks) and the mean value for the background counts (valley). The larger the peak to valley ratio, the better resolution is reached.

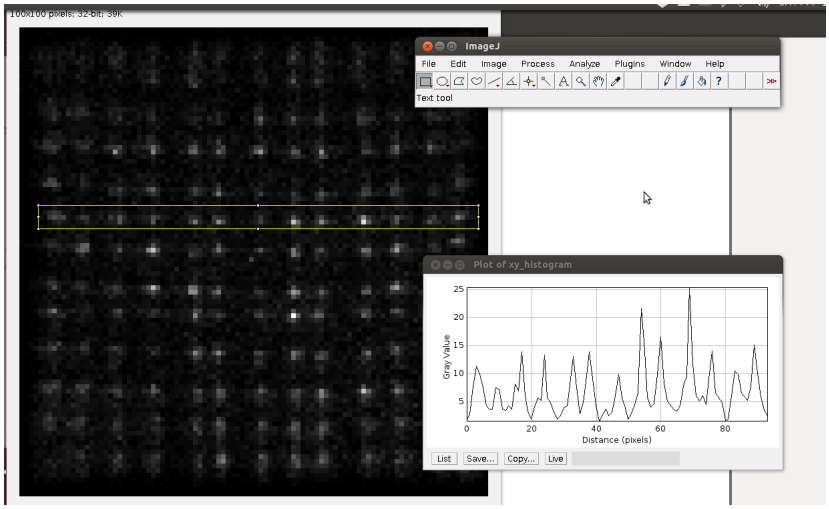

Figure 19: Scheme of the profile selection with program IMAGEJ.

By comparing the profile of a chosen row for different integration times an estimation of the optimum time can be done.

By looking at the plots in figure 20, the profile for t=100 and 150 ns shows a higher number of counts in the background which means that pile-up is distorting the data. This makes the peak to valley ratio much smaller so it can be concluded that the best integration time is one of the values 70-80-90 ns. However, it should be noted that the profiles for t=70,80,90 are very similar and it is quite difficult to affirm which is the best of them by looking at the plots. To be more precise the peak to valley is calculated and the results are presented in the following table.

integration time (ns)	90	80	70
peak to valley ratio	11.58	9.04	9.37

Table 2: Peak to valley ratio.

The three are very similar but the one for 90 ns seems to be the best.Therefore, the following analysis is done for integration times of 90 ns. Nevertheless, the results for 70 and 80 ns are also presented and compared in section 8.

[1]To be able to plot flood field maps with IMAGEJ it is necessary to create data file in binary code from a previous histogram of the variables x, y anger. This is done with a simple subroutine in the program $xyanger.f$, which creates output files with the form 'name'.bin.

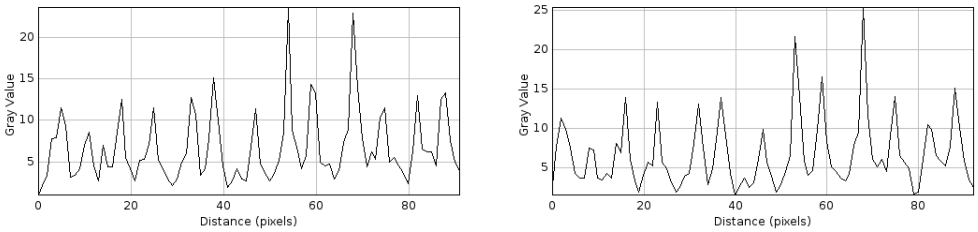

(a) 70 ns

(b) 80 ns

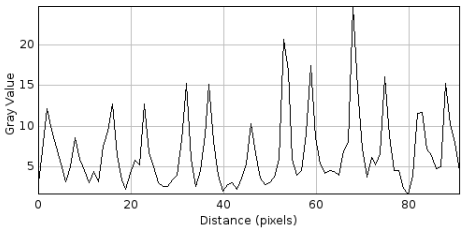

(c) 90 ns

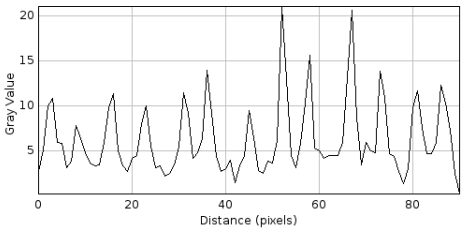

(d) 100 ns

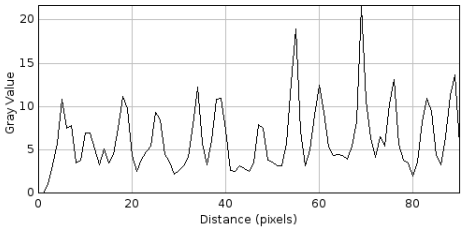

(e) 150 ns

Figure 20: Obtained profiles for a same row and for different integration times.

7.2. Phoswich separation. Delayed integration method

Once the integration time is fixed to the optimum value (90 ns in our case), the phoswich separation can be made, that is, it is possible to distinguish between LYSO and GSO counts. In order to make this partition, the *delayed energy integration method* is used. This method is based on the fact that materials which form the phoswich have different decay times.

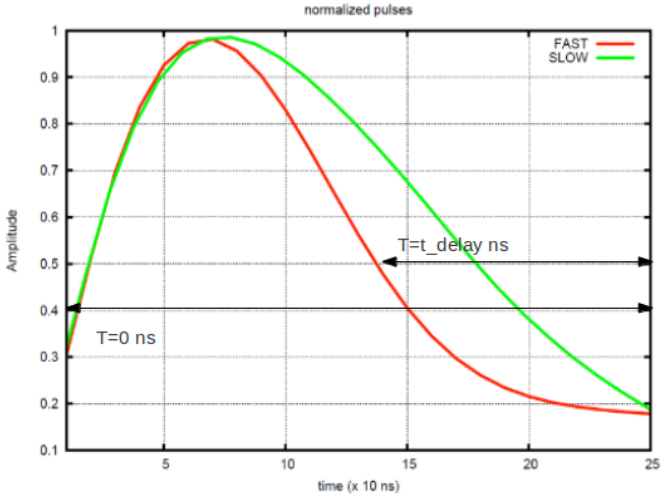

Figure 21: Average of 1000 LYSO pulses (red) and 1000 GSO pulses (green).The difference between decay times is clear and thus by integrating from $t > 0$ it is possible to distinguish between LYSO (less delay energy) and GSO (higher delay energy). Adapted figure from [2]

By integrating the pulses from a time bigger than zero (*delay time*) to the maximum integration time, it is obtained what is called *'delayed energy'*, which gives information about the layer (LYSO or GSO) where the interaction took place. The crystal with slower decay time would have a higher ratio of tail to total energy.

Indeed, as shown in Figure 21, larger delayed energy corresponds to materials with slower decay time. Thus, when plotting either delayed energy versus the total energy [2] or either the ratio $(\frac{delayed\ energy}{total\ energy})$ versus the total energy, counts in each layer can be separated and as a consequence the layer of interaction and a better estimation of the depth of interaction can be estimated.

In our particular case, LYSO has the faster decay having a 40 ns decay time and GSO the slow one with 60 ns, which means that the pulses with larger delayed energy correspond to interactions in GSO.

[2]Total energy is defined as the integrated energy when the pulse is integrated from time equal to zero

Again, the optimum value for the delay integration time must be found. This will give the best phoswich separation and thus reduce the uncertainty when determining the depth of interaction.

The procedure will be the same as in the previous section, the data is analyzed for several delay times and the plots are compared to find which gives the clearest separation.

Before presenting the plots some features about the way the plots are obtained must be pointed out:

- Figure 22(a) shows a plot where the total energy is represented as a function of the ratio. It can be noticed that counts seem to be divided in two regions. The left part would correspond to LYSO with faster decay and therefore smaller values for the energy ratio, and the right part would correspond to GSO counts.

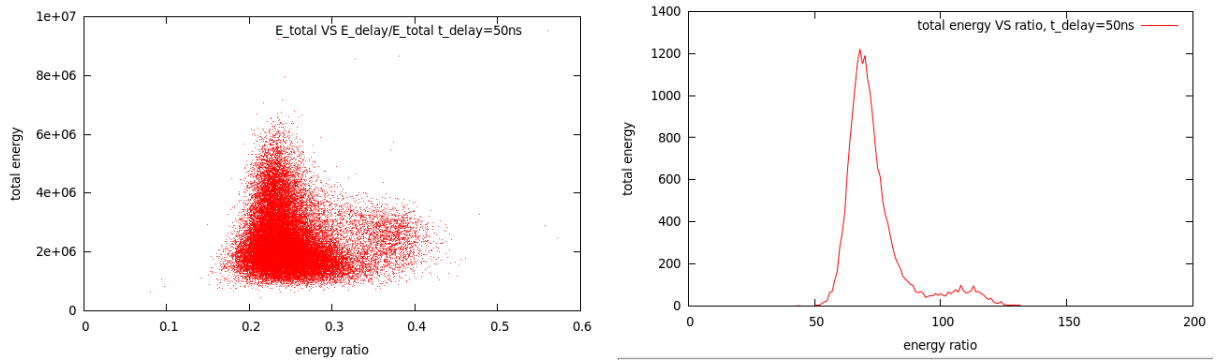

(a) (b)

Figure 22: (a)Total energy VS energy ratio ($ratio = \frac{E_{delay}}{E_{total}}$), (b)Re-scaled plot for total energy VS ratio.

However, from plots like the one in figure 22(a) it is impossible to separate accurately between the two different types of counts. In order to see a nice plot the axis must be rescaled. After finding a scale in accordance with our data the plots turn to be like in figure 22(b) where the separation is more clear.

- Other factor which has been taken into account is the background counts. At low energies the background becomes important in relation with the true counts because the energy difference between both is smaller. To minimize this possible error source, the lowest energy counts are ignored. Several plots are analyzed to find a reasonable value for the minimum energy at which the plots will be cut off. Since the number of counts is not very large, this energy threshold is set to a small value in order not to lose many counts.

Once the previous factors have been studied, the plots are ready to be compared to find the best delay time which gives the best layer separation. In the following, the results for different delays are presented.

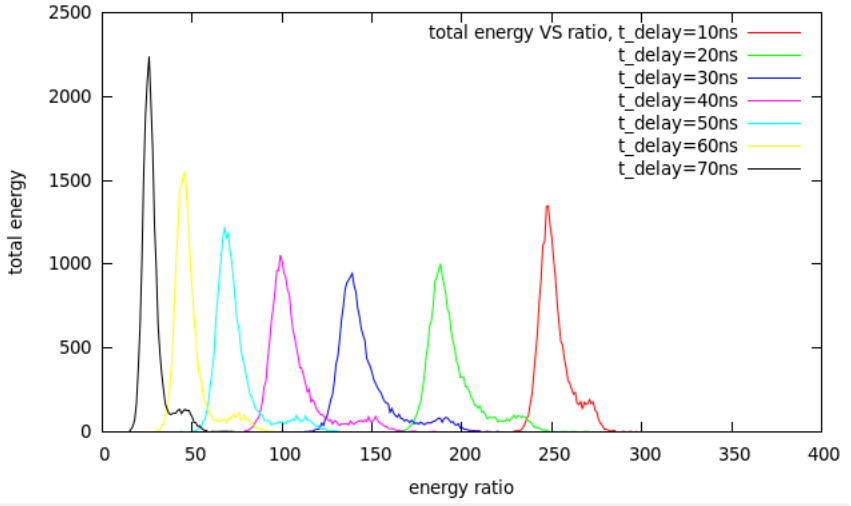

Figure 23: Total energy as a function of energy ratio for different delay times.

The best time delay is determined according to three main parameters:

- Distance between peaks, d. The higher distance between the two peaks the easiest will be to separate LYSO and GSO counts.

- Depth between the two peaks separation, Δx. A small depth will give a better separation.

- Energy resolution, as defined in previous sections, $FWHM = \frac{\Delta x}{E_\gamma}$. The smaller FWHM the better energy resolution. We work with FWHM for LYSO peak since the GSO peak is too small.

The distance between peaks is the most determining factor to make the partition. Then, by looking at the figure it can be inferred that the optimum value for the delay time would lay in between 20 ns and 50 ns which are the values for which the peaks are more distant. In order to compare dimensionless quantities, the comparison is made with the variables: $\frac{d}{FWHM}$ and $\frac{\Delta x}{h}$ where h is the height of LYSO peak.

The table shows the measured values for the parameters described above:

delay time (ns)	d	Δx	$FWHM(\%)$	h	$\frac{\Delta x}{h}$	$\frac{d}{FWHM}$
10	24	146	4.9	1343	0.011	4.9
20	46	62	9.0	997	0.062	5.1
25	50	45	11	920	0.048	4.5
30	53	47	12	917	0.051	4.4
35	55	47	13	928	0.050	4.23
40	53	43	14	1048	0.041	3.79
50	43	48	19	1185	0.040	2.27

Table 3: Parameters.

From the table, it can be concluded that the values which gives the best equilibrium for Δx, d and FWHM parameters are 25 ns.

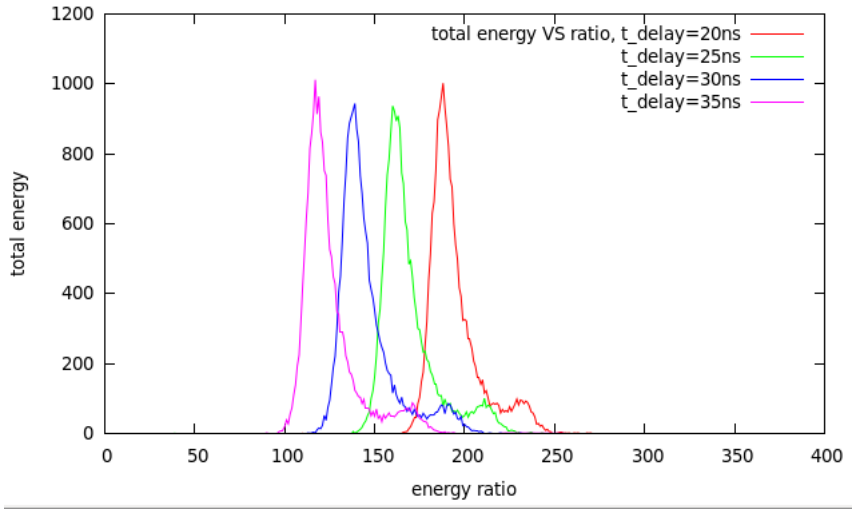

Figure 24: Total energy VS energy ratio detailed for 30, 35 and 40 ns.

Once an optimum delay time has been fixed, the next step is the separation of the two types of counts.

The separation point or **'phoswich limit' PL** will be set as the value for the energy ratio around the medium point between peaks and where the depth is smaller. The separation simply consists on taking the counts with ratio bigger than PL as GSO counts (right part in the figure) and those with smaller ratio as LYSO counts.

The partition is made with a simple FORTRAN program *'phoswich_total.f'* (SEE appendix A)

When separating the counts it is found that there are very few counts for GSO. This will be reflected in the flood field map and also in the spectra.

The very few number of GSO counts must be due to the detector is placed right in front of the source. That means that most of the counts interact in the first layer, LYSO, and very few interact with the second layer, GSO.

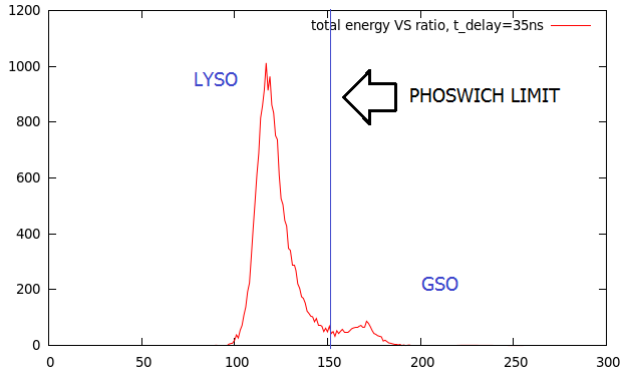

Figure 25: Total energy VS energy ratio for 35 ns.

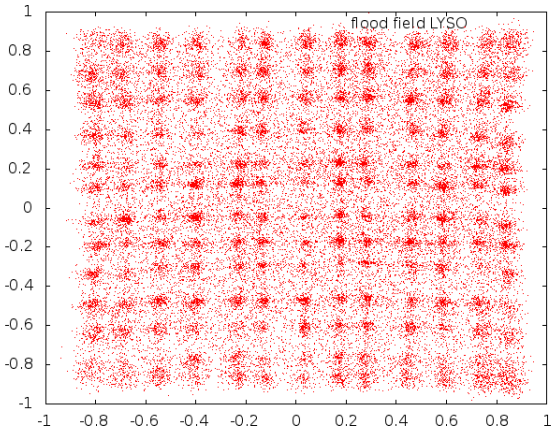

Figure 26: Flood field map for LYSO

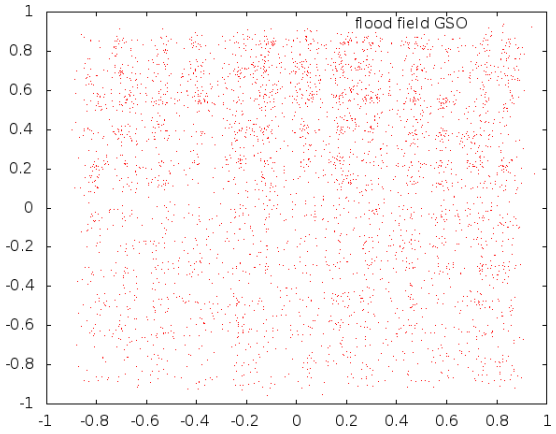

Figure 27: Flood field map for GSO

7.3. Crystal identification. Individual spectrum. Histogram and calibration.

Next task is to identify single crystals and plot the spectrum for all the counts which have interacted in it. By drawing on the flood field map (created with the program $xyanger.f$), the corners of a selected crystal can be known. Then, we look for the counts for which the x, y anger values are inside the interval enclosed by the corners. Afterwards, the corresponding energy for these counts is plotted and a histogram is made.

This is made with a FORTRAN program $'phoswich\_1crystal.f'$ where the input parameters are the x,y anger values for the corners. (see appendix A)

The steps followed are presented below:

1. The corners of a certain crystal are selected from the flood field map as shown in Figure 28.

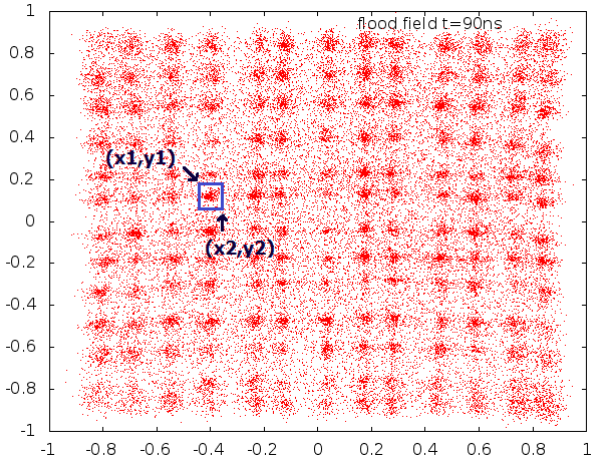

Figure 28: Crystal selection.In this example the crystal $6x4$ is selected. The crystal are labelled as $'rxc'$ where *'r'* is the raw number and *'c'* is the column number.

Those values for the corners (x_1, y_1, x_2, y_2) will be the input parameters for the program $phoswich\_1crystal.f$. By running this program, the counts inside the crystal are written in an output file (*fort.1*).

Figure 29 shows the histogram made from this output file for several crystals for LYSO and GSO counts.

2. Next task is to calibrate the counts obtained for the crystal, that is, to find the channel-energy relationship. As it was explained, this is essential to be able to sum up the individual spectra. Since every crystal has a different 'gain', each crystal will have different calibration factors.

In order to determine these calibration factors, we must find the channel which corresponds to the maximum number of counts(*'Chpeak'*). This is done by plotting an histogram for the counts in the crystal and associating 511 keV[3] to the channel corresponding to the maximum number of counts.
Moreover, the minimum energy is subtracted to the data. Thus the minimum channel can be associated to zero energy and the calibration line is given by:

$$E_{calibrated} = m \cdot E_{total} \tag{7}$$

[3]The value of 511 keV corresponds to the photo-peak for annihilation photons from the source used in the experiment, Sodium-22

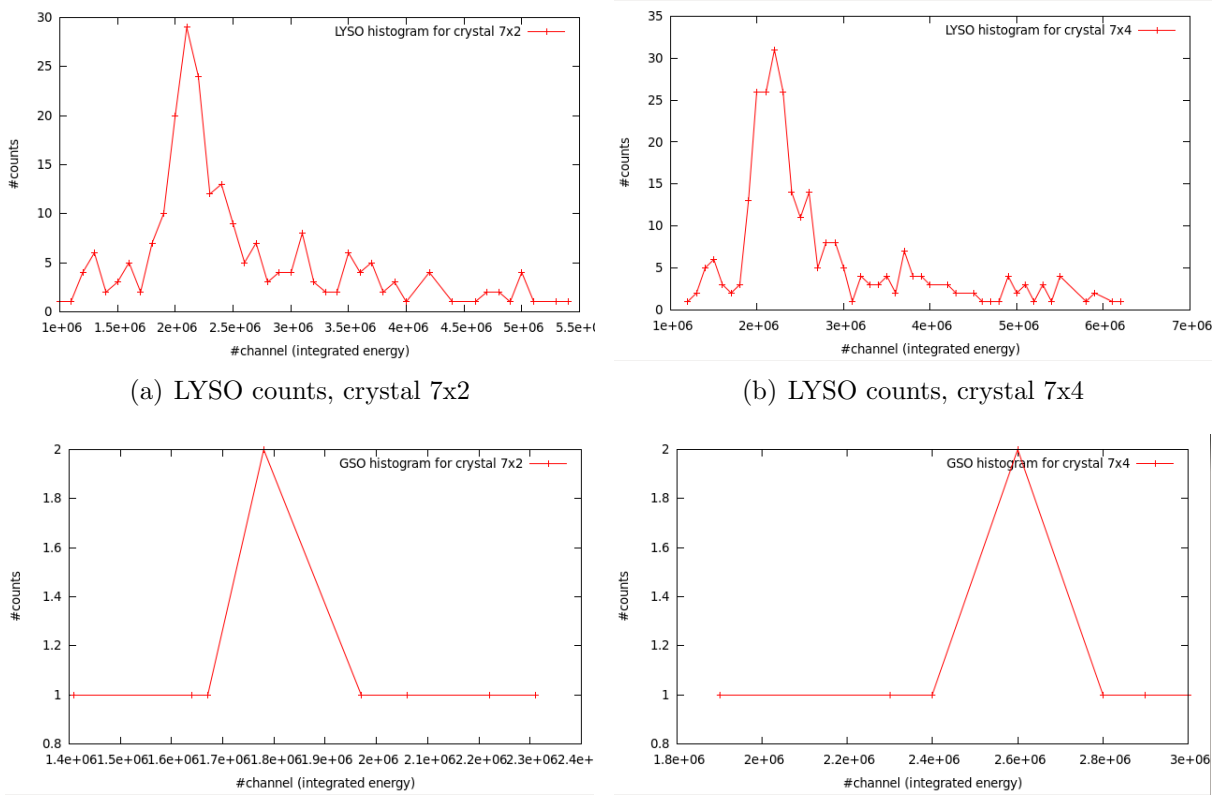

(a) LYSO counts, crystal 7x2

(b) LYSO counts, crystal 7x4

(c) GSO counts, crystal 7x2

(d) GSO counts, crystal 7x4

Figure 29: Histogram made from non-calibrated data for counts in LYSO and GSO crystals

where $m = \frac{511}{Chpeak}$.

Everything is done with program '*histo.f*' which gives an output file with the final calibrated data. This file can be plotted and again an histogram is made to study if the peak (maximum number of counts in the crystal) corresponds to 511 keV. Plots in figure 30 shows examples for these histograms and it can be observed how the peak appears around 500-510 keV.

3. Once the calibrated spectra have been obtained it is possible to sum up individual spectra for several crystals and obtain the total spectrum for LYSO and GSO with larger number of counts.
   For this purpose, the corners of around 50 crystals are taken from anger values and steps 1 and 2 are repeated for each case. Finally, we obtain a file with all the calibrated data for the crystals. The spectra in Figure 31 are obtained by plotting and making an histogram from this total data set. This is done automatically with the script *sum_spectra.sh*.

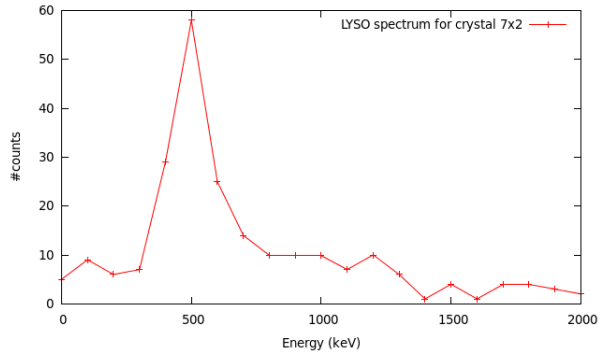

(a) LYSO spectrum, crystal 7x2

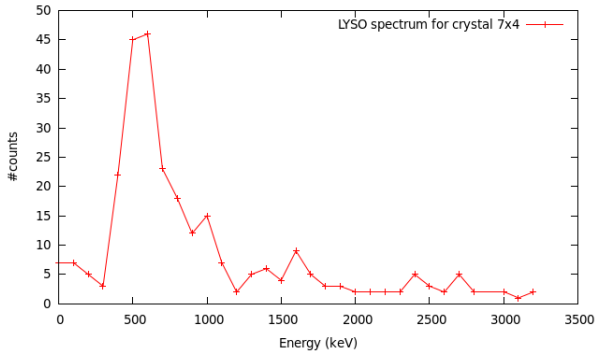

(b) LYSO counts, crystal 7x4

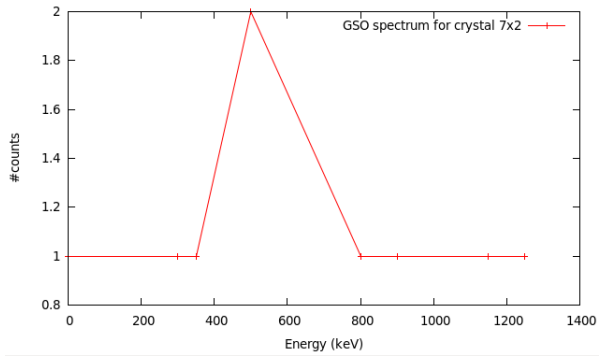

(c) GSO counts, crystal 7x2

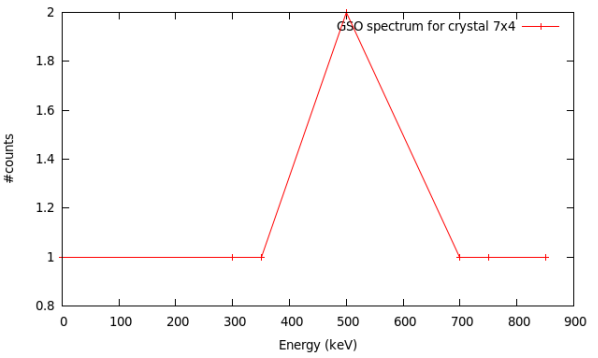

(d) GSO counts, crystal 7x4

Figure 30: Histogram made from calibrated data for counts in LYSO and GSO crystals.

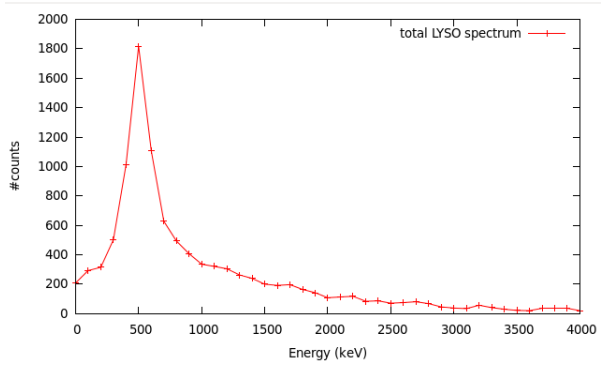

(a) LYSO total spectrum

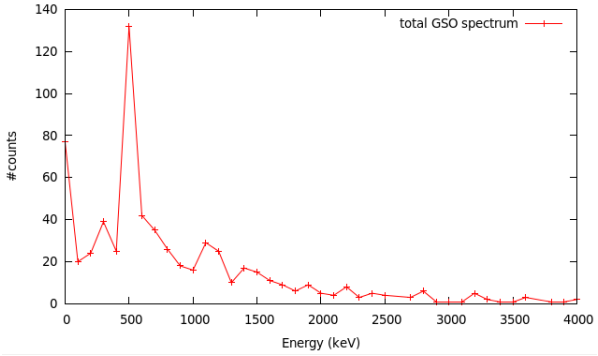

(b) GSO total spectrum

Figure 31: Histogram made from calibrated data for a large number of crystals. It can be observed that the photopeak appears around 500-510 keV as it was expected.

8. Comparison of results for different integration times

In section 7.1, the results for different integration times have been discussed. At the end, integration time equal to 90 ns had been taken as the best value since it was the one which gave the best peak to valley ratio and with higher number of counts. But from table 2 it can be noticed that the values for 70, 80 and 90 ns are very similar. Hence, the purpose of this section is to compare the final spectra[4] for these three values and confirm whether 90 ns is really the best value for the integration time or whether a better spectrum can be obtained with any of the two others (70 and 80 ns).

If the integration time is changed, the delay time may also change so the first step is to plot again the total energy versus the energy ratio to find the best delay time and phoswich separation.

Figure 32 shows that phoswich separation seems to be slightly more difficult for 70 ns since the second peak (GSO counts) is less clear. However, for 80 ns and 90 ns the plots are very similar and 25 ns looks like a good delay time.

Let us make the final spectrum for 80 ns and compare it with the one made for 90 ns. Figure 33 shows these spectra for 80 and 90 ns, it can be noticed how both spectra are very much the same.

9. Conclusions

From all the results and figures presented in the previous sections, it can be concluded that the best values for parameters which gives the best quality image for the data set analysed (array of 13x13 crystals of LYSO-GSO phoswich and Na-22 positron source) are $t_{integration} \approx 90ns$ and $t_{delay} \approx 25ns$. Small deviations for $t_{integration}$ from this value, inside the range 80-90 ns, have no important consequences for the final spectra. However, probably 90 ns holds as the best integration time.

The very few number of GSO counts is due to the detector being placed right in front of the source. That means that most of the counts interact in the first layer, LYSO, and very few are able to reach the second layer and interact with the GSO part.

[4]When talking about 'final spectra' we refer to the spectrum obtained by adding up all the individual spectra for a good number of crystals.

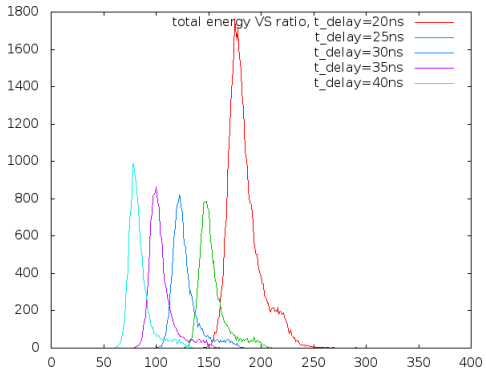

(a) integration time 70 ns

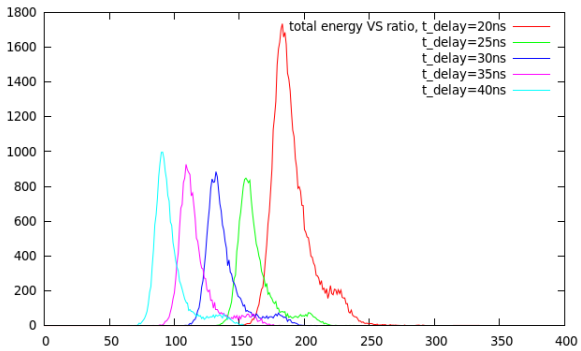

(b) integration time 80 ns

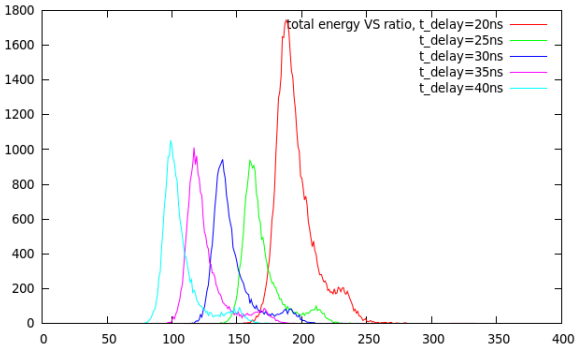

(c) integration time 90 ns

Figure 32: Total energy versus energy ratio for different integration times.

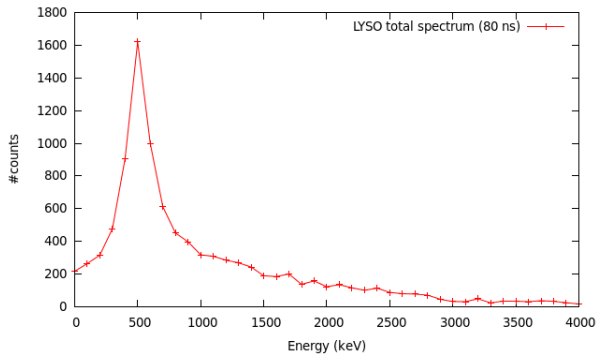

(a) LYSO total spectrum, 80 ns

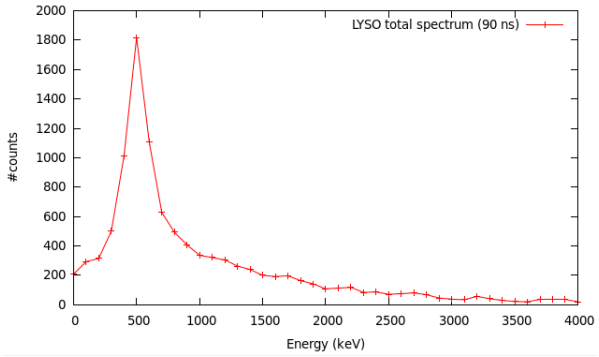

(b) LYSO total spectrum, 90 ns

Figure 33: Total spectra for integration time equal to 80 and 90 ns.

Other fact that must be noticed is the long tail for the final spectra, the spectra presented in figure 33, 31 are cut off around energy 4000 keV but actually the

counts in the original spectra reach higher energy. It is common to have counts for very high energy when rescaling spectra for crystals with very different gains. Moreover, since we use individual detectors instead of coincidence detections, the internal activity of Lutetium also contributes with high energy counts.

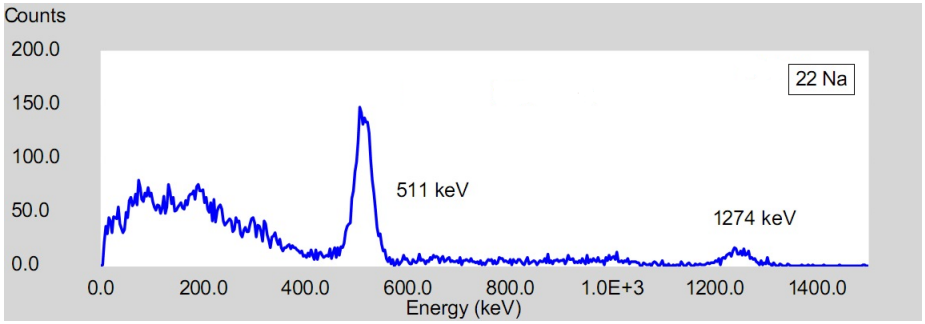

Figure 34: Real spectrum from a Na-22 source.

Regarding the second peak in Na-22 (around 1275 keVs, see figure 34), it is not visible due to the same reason, the number of counts is not enough to distinguish this second peak in the spectrum.

Apart from these two features (long tail and non-visible second peak), by comparing the obtained spectra (Figure 33,31) with the spectrum from a Na-22 source it can be concluded that the obtained spectra are fairly good.

From the study made in this work it can be concluded that *integration time* and *delay time* are two parameters which do have a big influence in the final layout of images in PET. On one hand, a good fitting for integration time contributes to reduce degrading factors like pile-up and entails a better identification of the crystal of interaction. On the other hand, when using phoswich technique, a proper value for delay time is needed to separate accurately the counts interacting in each phoswich layer. Therefore, those parameters must be studied to find the best values for each particular case (the values will depend on the material the phoswich is made of), and the electronics must be set-up according to those values.

A. Appendix

The aim of this appendix is to present in detail the programs used in this work. All the programs have been created in FORTRAN language.

A.1. $pulse - procesor.f$,

Author Jose Manuel Udías, adapted by the author of this work.

```
c234567
      program pulseprocesor

c     It is necessary to add this line because our
c     data set begins with a heading where the channels'
c     numbers are written: CANAL1  CANAL2  CANAL3  CANAL4.

      character*100 heading
      common iarr_samps(10000),n_samples,init_samples,n_delay
      integer ipmax, isamp, ipulse,i,j,npulses,imin,imax

      npulses=0
      ipmax=1000
c     initial samples for offset
      init_samples=10
      isamp=0
c     reading pulses, integrating and looking for a trigger point.
      ipulse_old=0
      imin=999999
      imax=-999999

c   reading the heading
      read(*,*)heading

      do 100 i=1,10000000
         do 100 j=1,1000000
c   reading the counts
            read(*,*,end=200)ipulse

            if(ipulse.eq.-1)then
               npulses=npulses+1
               n_samples=isamp
c              call the subroutine integrate(npulses,isamp)
               call integrate(npulses)
               isamp=0
c              writing in file 'fort.69', four columns:
               write(69,*)npulses,imin,imax,n_samples
               imin=9999999
               imax=-999999
               cycle
            endif
```

```
            isamp=isamp+1
            iarr_samps(isamp)=-ipulse

            if(imin.ge.ipulse)imin=ipulse
            if(imax.le.ipulse)imax=ipulse

 100      continue
 200      continue
          write(55,*)n_samples,imin,imax,npulses
          end

      subroutine integrate(npulses,isamp)

      common iarr_samps(10000),n_samples,init_samples,n_delay
      integer b_samps(10000),isum(8),ioffs(8),idel(8),sigmax

c     calculating offsets

      isumd=0
      do j=1,8
         isum(j)=0
         ioffs(j)=0
      enddo

      do 1000 is=1,init_samples
         ioffs(1)=ioffs(1)+iarr_samps(is)/init_samples

 1000 continue

      sigmax=-10000
      sigi=-10000.

c      looking for maximum total energy and peak, removing offsets
      sig_tot=0.d0
      amin=999999.
      amax=-999999.

      do 2000 is=1,n_samples
         b_samps(is)=iarr_samps(is)-ioffs(1)
         sig_tot=sig_tot+b_samps(is)
         if(b_samps(is).gt.sigmax)sigmax=b_samps(is)
         if(b_samps(is).lt.amin)amin=b_samps(is)
         if(sig_tot.gt.sigi)sigi=sig_tot
         write(37,*)npulses,is,b_samps(is)
 2000 continue
       amax=sigmax

c      CFD-like trigger point: marking at 10% of integral value

       itrig=0
       sig_tot=0.
```

```
       do 3000 is=1,n_samples

          do ic=1,1
             sig_tot=sig_tot+b_samps(is)
          enddo
          if(sig_tot.gt.0.005*sigi)then
             if(itrig.eq.0) ittrig=is
             itrig=1
          endif
 3000  continue

c       idel(*)=delay times
       idel(1)=-2
       idel(2)=10
       idel(3)=20
       idel(4)=30
       idel(5)=40
       idel(6)=50
       idel(7)=25
       idel(8)=35

c       ismax=integration time
       ismax=90

       do 3001 is=1,n_samples

c      if trig then integrate peaks upto n_samples

          if(is-ittrig.lt.ismax)then
             do 3002 i=1,8
                if(is-ittrig.gt.idel(i))then
                   isum(i)=isum(i)+b_samps(is)
                endif
 3002          continue
          endif
c          writing in 'fort.20' the integrated energy (isum) for
    different delay times (idel)
          write(20,'(i6,2i5,i6,8i8)')b_samps(is),is,ittrig,
     ,          sigmax,nint(sig_tot),isum(2),isum(3),isum(4),
     ,          isum(5),isum(6),isum(7),isum(8)
c      endif
 3001  continue
       write(21,'(i5,2i8,2e13.5,i5,7i8)')
     ,       sigmax,isum(1),ioffs(1),amin,amax,1,isum(2),isum(3),isum
    (4),
     ,       isum(5),isum(6),isum(7),isum(8)
       return
       end
```

A.2. *phoswich_total.f*

```
      program phoswich

c       input file: delay35_E_tot,ratio.txt
c       input parameter: value for phoswich limit (PL)
c       this file has five columns n_samples, E_total, ratio, xanger,
     yanger

       character*10 input1
       integer iargc,samp_GSO,samp_LYSO

       integer N
       parameter (N=100000)
       integer i,j,count
       integer n_sample(N)
       real E_total(N),ratio(N),x_anger(N),y_anger(N)
       real GSO(N),LYSO(N)

       real phoswich_limit
c      the value for the phoswich limit (PL) is selected from the plot

       real A(N,5)
c      opening two files, one for LYSO counts and other for GSO counts
       open(1,file='GSO_spectrum.txt')
       open(2,file='LYSO_spectrum.txt')

       nparam=iargc()

       if (nparam.lt.1)then
          write(*,*)'Introduce INPUT parameter: phoswich limit'
          stop
       endif

       call getarg(1,input1)
       read(input1,*)phoswich_limit

       phoswich_limit=phoswich_limit/300

       print*,'Phoswich limit is:', phoswich_limit

c      reading the input file:
       count=0
       do i=1,N
          read(*,*,end=100)(A(i,j),j=1,5)
          count=count+1
          n_sample(i)=A(i,1)
          E_total(i)=A(i,2)
          ratio(i)=A(i,3)
          x_anger(i)=A(i,4)
          y_anger(i)=A(i,5)
       enddo
```

```
 100   continue
       print*,count
       samp_GSO=0
       samp_LYSO=0
c      making the partition:
       do i=1,count
c         looking for counts with energy ratio bigger than PL (GSO
    counts)
          if (ratio(i).gt.phoswich_limit)then
             samp_GSO=samp_GSO+1
             GSO(i)=E_total(i)
c            writing GSO_spectrum.txt
             write (1,*)samp_GSO,GSO(i),ratio(i),x_anger(i),y_anger(i)
          endif
c         looking for counts with energy ratio smaller than PL (LYSO
    counts)
          if (ratio(i).lt.phoswich_limit)then
             samp_LYSO=samp_LYSO+1
             LYSO(i)=E_total(i)
c            writing LYSO_spectrum.txt
             write (2,*)samp_LYSO,LYSO(i),ratio(i),x_anger(i),y_anger(
    i)
          endif
       enddo

       print*,count,samp_GSO,samp_LYSO

       end
```

A.3. *xyanger.f*

```
  program Calculating x y anger

  integer nparam, iargc,nbin,ebin
  integer nbinmax,ebinmax
  integer Nevents
  parameter(Nevents=1000000,nbinmax=1000,ebinmax=1000)!,corrector
    =0.3)
     integer i,j,count,xA(Nevents),xB(Nevents),yA(Nevents),yB(Nevents)
  integer eee,nnn,ppp
  real x_anger(Nevents),y_anger(Nevents),total_energy(Nevents),xmax,
    ymax
  real xmin,ymin,deltaX,deltaY,deltaE,Emax,Emin
  real floodfield(nbinmax,nbinmax),histo(ebinmax)
  character*10 input1,input2
  character*200 filename1,filename2,filename3

  real A(Nevents,4)

c sets nparam to the number of command line arguments
```

```
  nparam=iargc()

  if (nparam.lt.1) then
        write(*,*) 'Introduce INPUT parameters'
        write(*,*) '1: Number of energy bins (ebin)'
   write(*,*) '2: Number of xy anger bins (nbin)'
   stop
  endif
c       reading input parameters
  call getarg(1,input1)
  read(input1,*)ebin
  write(*,*)'Number of energy bins:', ebin
  call getarg(2,input2)
  read(input2,*)nbin
  write(*,*)'Number of xy anger bins:',nbin
c opening common files (.txt)
  open(1,file='xy_anger.txt')
  open(2,file='xy_histogram.txt')
  open(3,file='E_histogram.txt')
  open(4,file='total_energy.txt')
c   declaring binary files (.bin) and opening them
c   binary files are needed to work with programs
c   like IMAGEJ or AMIDE
  filename1='xy_histogram.bin'
  filename2='E_histogram.bin'
  filename3='xy_anger.bin'
  call abrir(5,filename1)
  call abrir(6,filename2)
  call abrir(7,filename3)

  count=0
  do i=1,Nevents
c       reading input file
    read(*,*,end=100)(A(i,j),j=1,4)
    count=count+1
    yA(i)=A(i,1)
    yB(i)=A(i,2)
    xA(i)=A(i,3)
    xB(i)=A(i,4)
  enddo
100   continue

  xmax=-1000
  ymax=-1000
  xmin=1000
  ymin=1000
  Emax=-100000
  Emin=1000000

  do i=1,count
c       removing possible negative values for energy
     if ((xA(i).gt.1.0).AND.(xB(i).gt.1.0).AND.(yA(i).gt.
```

```
     P            1.0).AND.(yB(i).gt.1.0))then
c              calculatin x,y anger
         x_anger(i)=float(xA(i)-xB(i))/float(xA(i)+xB(i))
         y_anger(i)=float(yA(i)-yB(i))/float(yA(i)+yB(i))
         total_energy(i)=float(xA(i)+xB(i)+yA(i)+yB(i))

         write(1,*)x_anger(i),y_anger(i)
         write(7)x_anger(i),y_anger(i)
         write(4,*)total_energy(i)
c          calculating maximum an minimum values to make the histogram
    .
         if (x_anger(i).lt.-1.0)print*,x_anger(i)
         if (x_anger(i).gt.xmax) xmax=x_anger(i)
         if (x_anger(i).lt.xmin) xmin=x_anger(i)
         if (y_anger(i).gt.ymax) ymax=y_anger(i)
         if (y_anger(i).lt.ymin) ymin=y_anger(i)
         if(total_energy(i).gt.Emax) Emax=total_energy(i)
         if(total_energy(i).lt.Emin) Emin=total_energy(i)
      endif
   enddo

   print*, 'xmax = ', xmax
   print*, 'xmin = ', xmin
   print*, 'ymax = ', ymax
   print*, 'ymin = ', ymin
   print*, 'Emax = ', Emax
   print*, 'Emin = ', Emin
c calculating bin sizes
   deltaX=(xmax-xmin)/nbin
   deltaY=(ymax-ymin)/nbin
   deltaE=(Emax-Emin)/ebin

   print*, deltaX, deltaY, deltaE, nbin,ebin
c   calculating flood field map and energy histogram.
   do i=1,count
      nnn=int((x_anger(i)-xmin)/(deltaX+1e-12))+1
      ppp=int((y_anger(i)-ymin)/(deltaY+1e-12))+1
      eee=int((total_energy(i)-Emin)/(deltaE+1e-12))+1
      floodfield(nnn,ppp)=floodfield(nnn,ppp)+1
      histo(eee)=histo(eee)+1
   enddo

   do j=1,nbin
      do i=1,nbin
         write(2,*)i,j,floodfield(i,j)
         write(5) floodfield(i,j)
      enddo
   enddo
   do j=1,ebin
      write(3,*)j,histo(j)
      write(6) histo(j)
   enddo
```

```
  end

* ------------------------------------------------------
* ---------------- ABRIR  ------------------------------
*------------------------------------------------------

      Subroutine abrir(id,texto)

      Implicit none
      character*200 texto
      integer id

      Print *,'Opening..  ',texto
      write(*,*)
** INTEL
       Open(unit=id,file=texto,form='unformatted'
     + , recordtype='stream',carriagecontrol='none')

** ABSOFT
c        Open(unit=id,file=texto,form='unformatted')

       Return
      End
```

A.4. *phoswich_1crystal.f*

```
 program phoswich_singleCrystal

c     input file LYSO_spectrum.txt or GSO_spectrum.txt
c     input parameters, corners for the crystal:x1,x2,y1,y2

      character*10 input1,input2,input3,input4
      integer iargc,samples
      real x1,x2,y1,y2
      integer N
      parameter (N=100000)
      integer i,j,count
      real E_total(N),ratio(N),x_anger(N),y_anger(N),n_sample(N)
      real A(N,5)

      nparam=iargc()
c     input parameters:
      if (nparam.lt.1)then
         write(*,*)'Introduce INPUT parameters'
         write(*,*)'1: Coordinate x for upper corner (x1)'
         write(*,*)'2: Coordinate y for upper corner (y1)'
         write(*,*)'3: Coordinate x for bottom corner (x2)'
         write(*,*)'4: Coordinate y for bottom corner (y2)'
```

```
         stop
      endif

      call getarg(1,input1)
      read(input1,*)x1
      call getarg(2,input2)
      read(input2,*)y1
      call getarg(3,input3)
      read(input3,*)x2
      call getarg(4,input4)
      read(input4,*)y2

      print*,x1,y1,x2,y2
c     reading the input file:
      count=0
      do i=1,N
         read(*,*,end=100)(A(i,j),j=1,5)
         count=count+1
         n_sample=A(i,1)
         E_total(i)=A(i,2)
         ratio(i)=A(i,3)
         x_anger(i)=A(i,4)
         y_anger(i)=A(i,5)
      enddo
 100  continue
      samples=0

      do i=1,count
c     selecting counts inside the crystal
         if((x_anger(i).gt.x1).AND.(x_anger(i).lt.x2).AND.
     p         (y_anger(i).lt.y1).AND.(y_anger(i).gt.y2))then
            samples=samples+1
c           writing the counts inside the crystal in output file: '
   fort.1'
            write(1,*)E_total(i)
         endif
      enddo
      print*,samples

c     output file fort.1 --> E_total(i) in the selected crystal
      end
```

A.5. *histo.f*

```
      program histogram

c     input file fort.1, from phoswich_1crystal.f
c     input parameter, nbin=number of bins for the histogram

      character*10 input1
```

```
      integer iargc,samples
      parameter(N=1000)
      integer nbin,i,j
      real E_total(N),Emax,Emin,deltaE,channel(N),n_sample(N),Eoff(N)
      integer eee, histoE(N)
      real peak, Chpeak,E_cal,m,b,Chmin

      nparam=iargc()

      if (nparam.lt.1)then
         write (*,*) 'Introduce input parameter nbin'
         stop
      endif

      call getarg(1,input1)
      read(input1,*)nbin

      samples=0
c     reading input file fort.1 (counts in the crystal)
      do i=1,N
         read(*,*,end=100)E_total(i)
         samples=samples+1
      enddo
 100  continue

      Emax=0
      Emin=1000000000
c     looking for minimum energy
      do i=1,samples
         if(E_total(i).lt.Emin) Emin=E_total(i)
      enddo
c     subtracting the minimum energy to the data
      do i=1,samples
         Eoff(i)=E_total(i)-Emin
         write(7,*)Eoff(i)
      enddo
c     looking for maximum energy
      do i=1,samples
         if(Eoff(i).gt.Emax) Emax=Eoff(i)
      enddo
c     calculating bin size: deltaE
      deltaE=Emax/nbin

      print*,samples,Emax,Emin,deltaE

c     making the histogram
      do i=1,samples
         eee=int(Eoff(i)/deltaE)
         histoE(eee)=histoE(eee)+1
          write(4,*)eee,histoE(eee)
      enddo
```

```
      do i=0,nbin-1
         channel(i)=deltaE*i
c        write the histogram in fort.2
         write(2,*)channel(i),histoE(i)
      enddo

      peak=0
c     peak=maximum value for counts, from the histogram
      do i=1,nbin
         if(histoE(i).gt.peak)then
            peak=histoE(i)
c           Chpeak=channel corresponding to maximum value for counts.
            Chpeak=channel(i)
         endif
      enddo

      print*, peak, Chpeak

      m=511/Chpeak !m=calibration factor

      do i=1,samples
c        writing calibrated energy (E_cal) in file fort.3
         E_cal=Eoff(i)*m
         write(3,*)E_cal
      enddo

      print*, m

      end
```

A.6. *sum_spectra.sh*

```
for i in \$*
do

#input file: LYSO_spectrum.txt or GSO_spectrum.txt (from
    phoswich_total)

./phoswich_1crystal -0.44 0.018 -0.36 -0.095 <\$i> /dev/null

cp fort.1 \$i.spectrum_7x4
./histo 45 <fort.1> /dev/null
cp fort.2 \$i.histo_7x4
cp fort.3 \$i.calibration_7x4
rm fort.*

./phoswich_1crystal -0.72 -0.012 -0.64 -0.10  <\$i> /dev/null

cp fort.1 \$i.spectrum_7x2
./histo 45 <fort.1> /dev/null
```

```
cp fort.2 \$i.histo_7x2
cp fort.3 \$i.calibration_7x2
rm fort.*

cat \$i.calibration_7x2 \$i.calibration_7x4 ... > final.txt
```

References

[1] T.K.Lewellen,"The Challenge of Detector Designs for PET", *American Journal of Roentgenology*, vol.195, pp. 301-309, August 2010.

[2] J.J. Vaquero, J.J. Snchez, E. Lage, J.M. Udas, P. Guerra, M. Desco, "Design of DOI PET detector modules using phoswich and SiPMs: First Results" , *IEEE Nuclear Science Symposium Conference Record* October 2011.

[3] H. O. Anger, Scintillation camera with multichannel collimators *J.Nucl. Med.*, vol. 65, pp. 515531, 1964

[4] Krane K. S. 1987 Introductory Nuclear Physics (New York: Wiley)

[5] Knoll G F 2000 Radiation Detection and Measurements (New York: Wiley)

[6] Vicente Torrico, E. (2012) Caracterizacin, mejora y diseo de escneres PET preclnicos. Ph.D. Thesis. Universidad Complutense (Madrid)

[7] Espaa Palomares, S. (2009) Simulaciones avanzadas aplicadas al diseo de escneres y mejora de la calidad de imagen en tomografa por emisin de positrones . Ph.D. Thesis. Universidad Complutense (Madrid)

[8] Cal, J. Mejora de la identificacin del cristal de interaccin en escneres PET de alta resolucin mediante simulaciones . TAD Univesidad Complutense (Madrid)

[9] Ioannis G. Valais, Christos M. Michail, L. David, Anastasios Konstantinidis, Dionisis A. Cavouras, Ioannis S. Kandarakis and George S. Panayiotakis.," Luminiscence Emisision Properties of (Lu;Y)2SiO5:Ce (LYSO:Ce) and (Lu;Y)AlO3:Ce (LuYAP:Ce) Single Crystal Scintillators Under Medical Imaging Conditions", *IEEE Transactions on Nuclear Science*, Vol. 55, NO. 2, April 2008.

[10] C.S.Levin, E.J.Hoffman, "Calculation of positron range and its effect on the fundamental limit of positron emission tomography system spatial resolution", *Phys. Med. Biol.* vol.44, pp. 781799, 1999.

[11] http://en.wikipedia.org/wiki/Positron_ emission_ tomography

[12] http://gecommunity.gehealthcare.com/geCommunity/europe/nmpet/pet_ education/physics.html

[13] http://radiographics.rsna.org/content/19/1/155/F4.expansion.html

[14] http://en.wikipedia.org/wiki/Photomultiplier

[15] G.Tarantola, F.Zito, P.Gerundini, "PET Instrumentation and Reconstruction Algorithms in Whole-Body Applications", *J.Nucl.Med.*, vol.44, pp. 756-769, (2003).